TU Delft

Delft University of Technology

Groundwater-induced advective heat transfer in U-shaped closed-loop geothermal system application for a Red Sea rift sedimentary basin

Alobaid, Omar; Ezekiel, C. Justin; Daniilidis, Alexandros; Finkbeiner, Thomas; Mai, P. Martin

DOI
10.1186/s40517-025-00363-4

Publication date
2025

Document Version
Final published version

Published in
Geothermal Energy

Citation (APA)
Alobaid, O., Ezekiel, C. J., Daniilidis, A., Finkbeiner, T., & Mai, P. M. (2025). Groundwater-induced advective heat transfer in U-shaped closed-loop geothermal system: application for a Red Sea rift sedimentary basin. *Geothermal Energy*, *13*(1), Article 40. https://doi.org/10.1186/s40517-025-00363-4

Important note
To cite this publication, please use the final published version (if applicable).
Please check the document version above.

Copyright
Other than for strictly personal use, it is not permitted to download, forward or distribute the text or part of it, without the consent of the author(s) and/or copyright holder(s), unless the work is under an open content license such as Creative Commons.

Takedown policy
Please contact us and provide details if you believe this document breaches copyrights.
We will remove access to the work immediately and investigate your claim.

This work is downloaded from Delft University of Technology.
For technical reasons the number of authors shown on this cover page is limited to a maximum of 10.

Alobaid *et al. Geothermal Energy* (2025) 13:40
https://doi.org/10.1186/s40517-025-00363-4

Geothermal Energy

RESEARCH Open Access

Groundwater-induced advective heat transfer in U-shaped closed-loop geothermal system: application for a Red Sea rift sedimentary basin

Omar Alobaid[1*], C. Justin Ezekiel[2,3], Alexandros Daniilidis[4], Thomas Finkbeiner[1] and P. Martin Mai[1]

*Correspondence:
Omar.alobaid@kaust.edu.sa

[1] Physical Science and Engineering Division, King Abdullah University of Science and Technology, 23955-6900 Thuwal, Saudi Arabia
[2] Department of Earth, Energy, and Environment, Faculty of Science, University of Calgary, Calgary, Alberta T2N 1N4, Canada
[3] School of Public Policy, University of Calgary, Calgary, Alberta T2P 1H9, Canada
[4] Faculty of Civil Engineering and Geoscience, Reservoir Engineering, Delft University of Technology, Stevinweg 1, 2628CN Delft, the Netherlands

Abstract

This study investigates the thermal performance of closed-loop advanced geothermal systems under the influence of groundwater flow in deep sedimentary formations. By integrating advective heat transport into a 3D numerical model, we evaluate the combined effects of groundwater flow in deep sedimentary aquifers and geothermal heat transport and extraction using U-shaped closed-loop geothermal wells. The model is developed to simulate heat-transfer dynamics, incorporating well design with realistic casing and cement layers, layered geology with associated petrophysical uncertainties, and varying operational conditions. As study area, we selected the Midyan basin in Saudi Arabia, characterized by thick sedimentary formations and an elevated geothermal gradient. The results show that the advective heat transfer, induced by groundwater flow, significantly enhances system efficiency. Improvement in thermal power output increases by up to 27% over a 40-year operational period compared to conduction-only scenarios, particularly if groundwater flow is perpendicular to the lateral section of the wellbore. Sensitivity analysis reveals that geothermal gradient and reservoir depth are the most impactful geological parameters. Operational parameters such as injection rates (10—100 kg/s) and injection temperatures (25—45 °C) can be adjusted to further optimize the system performance, with 30 kg/s identified as the optimal injection rate that balances energy extraction and parasitic pumping losses. Well-design parameters, including diameters (0.114–0.245 m) and lateral length (0.5–3 km), also play a critical role, with longer lateral sections and larger diameters increasing the overall power output. These findings show the potential of U-shaped closed-loop advanced geothermal systems in sedimentary basins with dynamic groundwater flow and provide insights for optimizing geothermal energy systems in similar geological settings.

Introduction

One of the central challenges of this century is providing energy in a sustainable and affordable way to a growing global population while mitigating greenhouse gas emissions and reducing our dependence on fossil fuels. Despite global efforts to decarbonize the energy and with that the electricity sector, 60% of the electricity generation globally

Springer Open

© The Author(s) 2025. **Open Access** This article is licensed under a Creative Commons Attribution 4.0 International License, which permits use, sharing, adaptation, distribution and reproduction in any medium or format, as long as you give appropriate credit to the original author(s) and the source, provide a link to the Creative Commons licence, and indicate if changes were made. The images or other third party material in this article are included in the article's Creative Commons licence, unless indicated otherwise in a credit line to the material. If material is not included in the article's Creative Commons licence and your intended use is not permitted by statutory regulation or exceeds the permitted use, you will need to obtain permission directly from the copyright holder. To view a copy of this licence, visit http://creativecommons.org/licenses/by/4.0/.

is coming from fossil fuels (IEA 2023). As concerns over the depletion of finite natural resources and greenhouse emissions continue to rise, the need to adopt renewable and sustainable energy alternatives becomes more apparent (J. Wang & Azam 2024). Geothermal energy is a promising solution due to its continuous, low-carbon production of heat for direct-use applications such as space heating, cooling, and industrial processes. Importantly, because heating and cooling in many regions are provided through electricity, direct-use geothermal systems reduce electricity demand and thereby lower overall fossil-fuel consumption (Lund & Toth 2021; Pratiwi & Trutnevyte 2021; Ouerghi et al. 2024). Moreover, geothermal energy systems harvest the Earth's natural heat while having minimal environmental impact during production. Integrating geothermal systems into the energy mix enhances energy efficiency and reduces reliance on fossil fuels, making it a crucial part of the transition to cleaner energy systems, especially in countries like Saudi Arabia, where over 40% of electricity is generated from burning oil (Chettri & Sankarananth 2022; IEA 2023).

According to the classification by Moeck (2014), geothermal resources are broadly categorized based on the geological control into convection-dominated systems, typically represented by naturally fractured systems, enhanced geothermal systems (EGS), and conduction-dominated systems, such as those found in deep sedimentary basins or basement formation. Hydrothermal systems that rely on extracting hot water from underground aquifers have been widely studied and implemented (Ezekiel et al. 2022; Yu et al. 2023), including extensive uncertainty quantification studies (Wang et al. 2023). However, these systems often require treatment of produced water before re-injection, increasing operational costs and complexities (Kamila et al. 2021). Enhanced geothermal systems (EGS) have also gained attention, especially in geologic regions with low porosity and permeability. However, EGS rely on the creation of artificial fractures to facilitate heat exchange, which may lead to injection-induced seismicity (Majer et al. 2007; Kraft et al., 2009; Rathnaweera et al. 2020; Zang et al. 2014). In recent years, there has been increasing interest in closed-loop geothermal systems (CLGS), also called Advanced Geothermal Systems (AGS) (Beckers et al. 2022; Malek et al. 2022). These systems are unique because they work without directly interacting with aquifer brines, which reduces scaling/corrosion issues and contamination risks. This makes them easier to use in a wider range of geological settings, although often with a lower power output when compared with conventional open-loop systems (Yuan et al. 2021; White et al. 2024).

The performance of geothermal systems is influenced by several factors, including geological conditions (Schill et al. 2016), operational and design parameters, and economics (Daniilidis 2024). The previous research on CLGS has often focused on hot dry rock, where heat transfer occurs only through heat conduction (Beckers et al. 2022; Huang et al. 2024; Song et al. 2018; White et al. 2024). In deep sedimentary aquifers, the groundwater flow governed by hydraulic head and conductivity introduces an advective component to the heat exchange process that must be accounted for (Yolcubal et al., 2004; Liu et al., 2024). These sedimentary aquifers generally consist of either siliciclastic (e.g., sandstone, conglomerate, or mud rocks) or carbonate rocks (e.g., calcite and dolomite). The lithological composition of these rock types as well as their hydraulic and thermal conductivities directly affect the heat transfer of such geothermal systems (Maliva, 2016).

In this context, Diao et al. (2004) established a conduction–advection equation to solve for the heat transfer in ground heat exchangers in the presence of groundwater flow. Hecht-Mendez et al. (2013) optimized an array of shallow vertical borehole heat exchangers (BHEs) using numerical simulation, showing an improvement in heat transfer when considering groundwater flow. A recent study by Brown & Falcone (2025) investigated the influence of groundwater flow direction on the thermal performance of single and multi-lateral U-shaped advanced geothermal systems. However, the combined effects of geological, operational, and design parameters, such as formation properties, injection conditions, and wellbore configuration, in advective regimes remain underexplored.

This raises several key questions: (1) How does advective heat transport influence the efficiency and long-term performance of U-shaped CLGS in sedimentary basins? (2) What are the geological and operational parameters that govern the system performance under dynamic hydrological conditions? (3) How can wellbore design and material properties be optimized to maximize heat transfer efficiency and overall system performance? Addressing these questions is critical for evaluating CLGS viability as a geothermal energy solution.

Our study integrates groundwater flow into the heat transfer model to provide a comprehensive understanding of the performance of U-shaped CLGS under dynamic hydrological conditions. The 3D physics-based model presented in this paper accounts for conduction and advection by incorporating varying formation properties and groundwater flow magnitude and direction to simulate real-world geological conditions. The U-shaped wellbore is represented by a verified 1D line source that incorporates multiple layers of casings and cement and accurately simulates heat transfer from the reservoir to the wellbore and from there to the working fluid. The system's performance is quantitatively evaluated using key metrics such as net power (MW), cumulative thermal energy output (MJ), and temperature profiles. Furthermore, we conduct a local sensitivity analysis to determine the impact of geological and operational parameters on the performance of the U-shaped CLGS.

Methodology

We model both conductive and advective heat transfer to assess the impact of groundwater flow on CLGS performance. With a commercial finite element analysis software we simulate the heat transfer process between the formation and the working fluid flowing through wellbore. The methodology section provides the governing equations for fluid flow and heat transfer. We also present an overview of the geological context of the study area (Midyan basin), a coastal area located in northwestern Saudi Arabia, followed by a description of the study setup which includes key parameters, systems configuration, and groundwater flow conditions. Lastly, we summarize the numerical model covering model geometry, performance metrics, mesh analysis, and sensitivity analysis to quantify the influence of key geological, operational, and design parameters on the system performance.

Governing equations

The continuity and momentum equations for fluid flow in the pipe are expressed as (Barnard et al. 1966)

$$\frac{\partial A\rho_f}{\partial t} + \nabla \cdot \left(A\rho_f u\right) = 0 \tag{1}$$

This equation ensures mass conservation within the wellbore. In Eq. 1, A is the cross-sectional area of the pipe(m^2), ρ_f is the working fluid density(kg/m^3), u and is the velocity of the working fluid(m/s). This equation ensures mass conservation within the wellbore. The momentum equation governs the forces acting on the fluid and can be expressed as:

$$\rho_f \frac{\partial u}{\partial t} + \rho_f u \cdot \nabla u = -\nabla p - f_D \frac{\rho_f u|u|}{2d_h} + F \tag{2}$$

where p is the pressure (Pa), f_D is the darcy friction factor, d_h is the hydraulic diameter (m), and F is the volume force term (N/m^3). The hydraulic diameter, d_h, can be defined as:

$$d_h = \frac{4A}{Z} \tag{3}$$

where Z is the wetted perimeter of the pipe (m).

For single-phase fluids, the Churchill equation can be used to determine the Darcy friction factor f_D across the full range of Reynolds numbers (Re) (Churchill 1977)

$$f_D = 8\left[\left(\frac{8}{Re}\right)^{12} + (A+B)^{-1.5}\right]^{1/12} \tag{4}$$

$$A = \left[-2.457 \ln\left(\left(\frac{7}{Re}\right)^{0.9} + 0.27\left(\frac{e}{d}\right)\right)\right]^{16} \tag{5}$$

$$B = \left(\frac{37530}{Re}\right)^{16} \tag{6}$$

where A and B are empirical constants, e is the absolute pipe roughness (m), and d is the hydraulic diameter (m).

In the laminar flow regime (Re < 2000), the Darcy friction factor f_D is independent of surface roughness and can be approximated by the Stokes formula:

$$f_D = \frac{64}{Re} \tag{7}$$

The energy equation for incompressible fluid flow in a pipe is expressed as follows (Lurie 2008):

$$\rho_f A C_p \frac{\partial T}{\partial t} + \rho_f A C_p u \cdot \nabla T_f = \nabla \cdot \left(A\lambda \nabla T_f\right) + f_D \frac{\rho_f A}{2d_h}|u|^3 + Q_{wall} \tag{8}$$

The terms on the left-hand side of the energy equation account for the change of thermal energy in the fluid and the convective heat transport. On the right-hand side, the equation captures the conductive heat transfer, viscous dissipation, and heat exchange rate. In Eq. 8, ρ_f represents the working fluid density $\left(kg/m^3\right)$, A is the cross-sectional area of the pipe (m^2), C_p is the heat capacity $J/\left(kg \cdot K\right)$, T is the temperature K, and u represents the velocity of the fluid. The term λ is the thermal conductivity $(W/(m \cdot K))$. Q_{wall} refers to the conductive heat transfer through the pipe wall.

Following Coulson et al., (1990), the radial heat transfer from the surrounding domain into the pipe is expressed as:

$$Q_{wall} = (hZ)_{eff}(T_{ext} - T) \tag{9}$$

where $(hZ)_{eff}$ is the effective heat transfer coefficient, T_{ext} is the external temperature of the formation, and T is the temperature of the fluid. The temperature coupling between the fluid inside the pipe and the surrounding domain is modeled as a line heat source, where the source strength is proportional to the temperature difference between the pipe fluid and the surrounding material. In this formulation, the line heat source serves as a computationally efficient representation of the wellbore, while the impact of the multiple casing and cement layers are captured through the effective heat transfer coefficient $(hZ)_{eff}$, given as

$$(hZ)_{\text{eff}} = \frac{2\pi}{\sum_{i=1}^{N}\left(\frac{\ln\left(r_{i+1}/r_i\right)}{\lambda_i}\right) + \frac{1}{r_{\text{int}}h_{\text{int}}} + \frac{1}{r_{\text{ext}}h_{\text{ext}}}} \tag{10}$$

In Eq. 10, N is the number of concentric layers, r_i and r_{i+1} are the inner and outer radii of layer i, and λ_i is the thermal conductivity of layer i(W/(m·K)). The terms r_{int} and h_{int} represent the inner radius and internal convective heat transfer coefficient, respectively, while r_{ext} and h_{ext} are the radius and external heat transfer coefficient for the formation.

The heat transfer in a saturated reservoir is described by the advection–diffusion equation (Nield & Bejan 2017)

$$\rho_f C_{p,f} u_w \cdot \nabla T + \left(\rho C_p\right)_{\text{eff}} \frac{\partial T}{\partial t} = \lambda_{\text{eff}} \nabla^2 T + Q_E \tag{11}$$

In this equation, ρ_f is the fluid density in the reservoir (kg/m3), $C_{p,f}$ is the specific heat capacity of the fluid (J/(kg·K)), and u_w is the Darcy velocity (m/s), representing the groundwater flow in the porous medium. The effective volumetric heat capacity $\left(\rho C_p\right)_{\text{eff}}$ is defined as:

$$\left(\rho C_p\right)_{\text{eff}} = (1-\phi)\rho_r C_{p,r} + \phi \rho_f C_{p,f} \tag{12}$$

where ϕ is the porosity of the rock, ρ_r and $C_{p,r}$ are the density and heat capacity of the rock matrix, respectively. The effective thermal conductivity λ_{eff} is defined as

$$\lambda_{\text{eff}} = (1-\phi)\lambda_r + \phi \lambda_f \tag{13}$$

with λ_r and λ_f being the thermal conductivities of the rock matrix and fluid, respectively. The term Q_E balances the line-sink term in Eq. 8 and together they form a source–sink pair that conserves energy between the wellbore and the surrounding formation.

Study area

The Midyan basin, located along the northwestern margin of Saudi Arabia, forms part of the tectonically active Red Sea Rift system and represents a prime target for geothermal energy exploration due to its elevated heat flux (70–90 mW/m2) associated with tectonic activity (Limberger et al. 2018; Lucazeau 2019) (Ezekiel et al. 2022; Yalcin et al 2024). Owing to its thick sedimentary formations, the Midyan basin offers favorable conditions to study the role of groundwater flow and advective heat transport in CLGS (Hughes & Johnson 2005). In particular the Oligocene Al Wajh formation is a primary focus of this study due to its significant depth (as deep as 5000 m) and a favorable geothermal gradient of 30—40 °C/km. Moreover, projected economic development and tourism growth in this area, driven by major projects such as NEOM[1] will increase demands for electricity, cooling, heating (Ürge-Vorsatz et al. 2015), and desalination (Gössling et al. 2012; Gude 2016).

Figure 1a depicts the generalized lithostratigraphy of the Midyan basin. The Al Wajh Formation is bounded by sequences of interbedded carbonates, evaporites, clastic sediments, and basement. This geologic structure creates a complex but favorable geological environment for heat transfer. Figure 1b depicts the study area's location along the Red Sea including the seismic cross-section line (A–A').

Study setup

Our simulations are designed to cover a range of geological and operational parameters to evaluate how their variabilities and uncertainties influence thermal output. The goal is to identify key factors that govern both conductive and advective heat transfer, which may provide insights for optimizing the system's performance. These include variations in groundwater flow velocity, formation properties (e.g., thermal conductivity, geothermal gradient, porosity, and permeability), and operational/design parameters (e.g., injection rate and temperature, wellbore diameter, lateral length, and material selection). The "base-case" parameters, such as wellbore dimensions, the formation's petrophysical and thermal properties, as well as operational parameters are summarized in Table 1.

The model assumes a single-phase flow of the working fluid within the wellbore, which is rate-controlled for both injection and production. Both the injection rate and temperature are assumed to remain constant throughout the simulation. Heat transfer via radiation and phase transitions of the working fluid are considered negligible due to the operational conditions. In addition, the model incorporates groundwater flow within the target formation, driven by a regional pressure gradient across the sedimentary layer to account for advective heat transport effects. We consider multiple scenarios of

[1] NEOM is an acrology located in Saudi Arabia's Tabuk province bordering the Red Sea and Gulf of Aqaba. It consists of several so-called giga projects including a floating industrial complex, a global trade hub, tourist resorts and a linear city. These projects rely on a sustainable, renewable energy concept including the development and exploitation of geothermal heat.

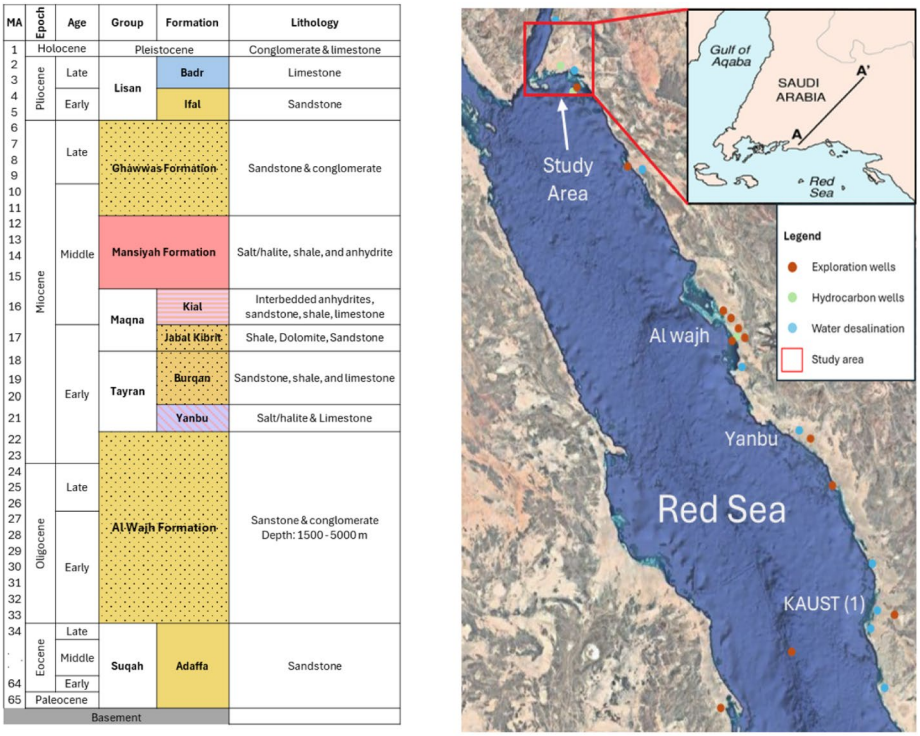

(a) (b)

Fig. 1 **a** Generalized lithostratigraphy of the Midyan basin, highlighting the Al Wajh Formation as our target horizon. **b** Map showing the study area (upper right) as well as locations of exploration wells and water desalination plants along the Red Sea. The A–A′ in the upper right corner is a seismic line used to interpret subsurface geology. (Modified from Hughes & Johnson 2005; Tubbs et al. 2014; Ezekiel et al. 2022)

Table 1 Base case parameters and key parameters for CLGS evaluation

Parameter	Value	Range	Unit
Lateral length (L_h)	2000	500–3000	m
Reservoir depth (z)	5000	3000–5000	m
Geothermal gradient (G)	32	25–40	°C/km
Wellbore inner diameter (ID)*	0.178	0.114–0.245	m
Inlet fluid temperature (T_{in})	35	20–40	°C
Injection rate (m)	20	10–100	kg/s
Formation thermal conductivity (λ_r)	3.1	2.84–3.72	W/(m·K)
Porosity (ϕ)	0.15	0.05–0.2	–
Permeability (k)	50	–	mD
Darcy velocity (u)	20	0–20	m/yr
Specific heat capacity of formation ($C_{p,r}$)	1000	–	J/(kg·K)
Heat capacity of fluid ($C_{p,f}$)	4181	–	J/(kg·K)
Fluid density (ρ_f)	1000	–	kg/m^3
Rock density (ρ_r)	2600	–	kg/m^3
Pump efficiency (η)	0.75	–	–

groundwater flow in this study including variations in flow velocity and direction relative to the lateral section of the wellbore (e.g., perpendicular versus parallel alignments).

Figure 2 shows the setup of the U-shaped CLGS, which consists of two main components: the formation and the wellbore. The target formation is a deep sedimentary aquifer within the Al Wajh formation sealed by interbedded low permeability evaporites, shale, and salt layers at the top, and impermeable basement rock at the bottom. These layers restrict groundwater flow to the horizontal direction and drive advective heat transport within the target formation. The wellbore configuration consists of two main sections: an injection well with an extended lateral section, and a vertical production well that intersects the end of the lateral section to form a U-shaped geometry. The lateral section of the injection well resides in the deep sedimentary aquifer and captures the advective heat transport. Our model also considers realistic well construction with multiple hole sections and associated casing sizes and cement sheaths (respective dimensions are listed in Table 2). Inclusion of accurate well design is necessary to accurately capture heat transfer between the penetrated formations and working fluid (Song

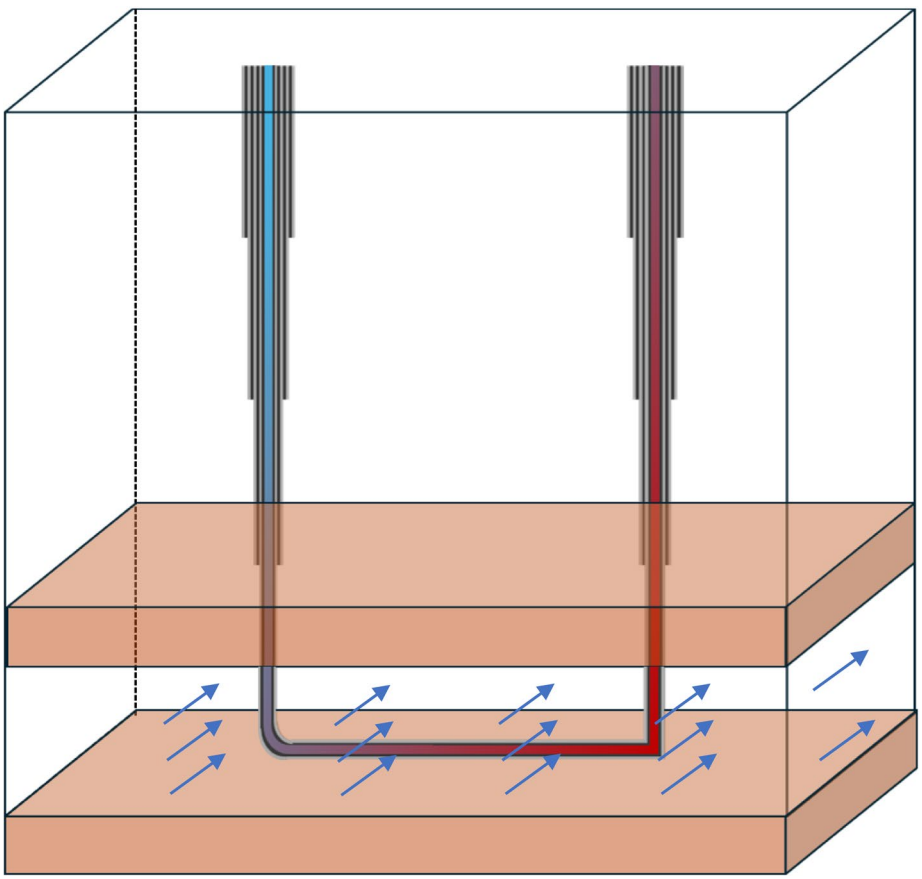

Fig. 2 Schematic of a U-shaped closed-loop geothermal system (CLGS). The wellbore configuration consists of two main sections: a horizontal injection well with an extended lateral Sect. (2000 m), and a vertical production well (5000 m) that intersects the end of the lateral section. The lateral section of the wellbore is located in a dynamic groundwater aquifer. The groundwater flow facilitates advective heat transfer which enhances the system. The schematic is not drawn to scale

Table 2 Wellbore dimensions and thicknesses of casing and cement layers of varying sections (conversion factor from SI to English units: 1 in = 0.0254 m)

Drilling diameter (m)	Casing diameter (m)	Total thickness (m)*	Depth (TVD) (m)
0.914	0.762	0.737	1000
0.610	0.508	0.432	2000
0.445	0.340	0.267	3000
0.311	0.245	0.133	4000
0.216	0.178	0.038	5000

*The total thickness of the wellbore is the difference between the inner diameter of the pipe and the outermost diameter

Table 3 Thermal conductivity (W/m•K) values for wellbore materials

Material	Thermal conductivity
Casing	40
Thermally conductive cement	0.8
Insulating material	0.05

et al. 2018). The working fluid, water, is injected at constant temperature and circulated at constant rate.

Numerical model setup

Model geometry

A 3-D model with dimensions of 5000 m × 1000 m × 5600 m is constructed to capture the relevant geological formations and thermal properties needed to parameterize the heat transfer dynamics in a CLGS. The geological domain comprises a sequence of homogeneous layers to which layer-specific values for thermal conductivity, porosity, and permeability are assigned. We include overburden and basement strata to simulate subsurface conditions anticipated for the Midyan basin geology. These can be adapted to similar syn–rift sedimentary basin settings in future work.

The target sedimentary formation is located at a depth interval between 4 and 5 km. A regional differential pore pressure of 1.5 MPa is applied across this sedimentary layer to drive groundwater flow, allowing the model to capture the effects of advective heat transport. We assume no-flow boundary conditions at the top and bottom to force horizontal groundwater flow, a constant Darcy velocity across the reservoir domain, and a fixed far-field temperature corresponding to the formation temperature from the geothermal gradient.

The U-shaped wellbore is represented as a line source consisting of three connected sections: a vertical downhole injection segment, a horizontal lateral segment, and a vertical uphole production segment. The lateral segment, extending 2000 m within the sedimentary layer, is aligned normal to the groundwater flow to maximize advective heat transfer. Three different materials comprise the wellbore: casing, thermally conductive cement, and insulating layer. The insulation layer is applied to the upper part of the production well, extending from the surface to a depth of 1 km, to minimize thermal losses

in the shallow region. The thermal conductivities of these materials are presented in Table 3.

Performance metrics

The performance of the closed-loop geothermal system (CLGS) is evaluated using the thermal energy extracted during operation and the cumulative thermal energy over the simulation period. The thermal energy at any given time, $P(t)$, is determined as

$$P(t) = \dot{m} \cdot c_p \cdot \left(T_{out}(t) - T_{inj}\right) \tag{14}$$

where $\dot{m}$ is the mass flow rate of the working fluid (kg/s), c_p is the specific heat capacity of the fluid, T_{out} is the fluid outlet temperature, and T_{inj} is the injection temperature. This metric reflects the gross power being extracted from the system. For the energy consumed by the pumping process, the parasitic pump power, P_{pump}, is subtracted from the gross power to produce the net power output

$$P_{pump}(t) = \frac{\dot{m} \cdot \Delta \mathrm{p}}{\rho_w \cdot \eta_{pump}} \tag{15}$$

$$P_{net}(t) = P(t) - P_{pump} \tag{16}$$

where Δp is the pressure drop between the injector and producer, and η_{pump} is the pump efficiency with a value of 0.75. The cumulative thermal energy, E_{total}, is calculated by integrating the net power output over the simulation period

$$E_{total} = \int_0^{t_{op}} P_{net}(t)dt \tag{17}$$

where t_{op} is the total operational duration. This metric measures the total energy produced by the system and provides a comprehensive view of its long-term performance under varying operational and geological conditions.

In addition to the energy output, the influence of advective heat transfer is characterized by the Peclet number (Pe), defined as (Bear 1972; Huysmans & Dassargues 2005)

$$P_e = \frac{u \cdot L}{\alpha_T \cdot u + D_0} \tag{18}$$

where u is the effective groundwater velocity, L is the characteristic length (wellbore diameter), α_T is the transverse dispersion, and D_0 is the molecular diffusion. This dimensionless parameter (P_e) quantifies the relative contribution of advective heat transfer over conductive heat transfer. By using this parameter, we simulate the transition from conduction-dominated to advection-dominated regimes.

Finally, to evaluate the influence of key parameters on system performance, a local sensitivity analysis is conducted. Selected parameters are varied by $\pm 15\%$ relative to their base-case values, and the resulting changes in the cumulative thermal energy are analyzed. The sensitivity coefficient (α) of each parameter is quantified using the following equation

$$\alpha = 100 \times \frac{E_{\text{high}} - E_{\text{low}}}{30 \cdot E_{\text{base}}} \tag{19}$$

in which E_{high} and E_{low} represent the cumulative thermal energy at + 15% and − 15% variations of the parameter, and E_{base} is the cumulative thermal energy under base-case conditions. A higher sensitivity coefficient indicates that small changes in the parameter results in larger variation in the energy output.

Validation

To validate the accuracy of our physics-based model, we reproduced the conduction-only scenario of Ghassemi & Zhang (2004). Their study provides a benchmark for heat transfer in closed-loop borehole systems, including wellbore geometry, thermal conductivity of the wellbore, formation properties, and injection rate. Using their input parameters, we simulated the temperature profiles in COMSOL and compared the results with the published analytical solutions.

Figure 3 shows the radial temperature distribution at different times, expressed as a function of normalized distance r/R from the wellbore, where r is the radial distance and R is the wellbore radius. The simulation results confirm that the model accurately captures the heat transfer between the wellbore and formation.

Mesh sensitivity

Mesh refinement around the wellbore is essential to accurately capture heat transfer from the formation to the working fluid inside the wellbore. The model is meshed using tetrahedral elements to resolve the geometry (Fig. 4). Different meshing schemes are tested to balance accuracy and computational time. The baseline mesh resolution is set to one element per meter along the wellbore (e.g., mesh refinement × 1). The mesh density is varied from 0.5 to 20 element per meter.

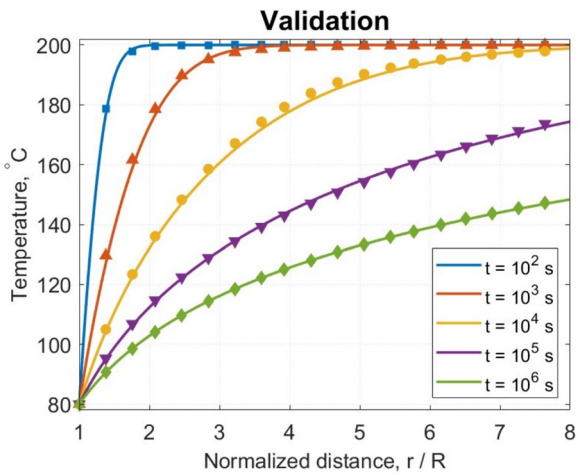

Fig. 3 Comparison of simulated temperature distribution (lines) with the benchmark results of Ghassemi & Zhang (2004) (symbols) for different times (10^2–10^6 s). the radial temperature profiles are plotted as a function of normalized distance (r/R) from the wellbore. The close agreement confirms the accuracy of our model

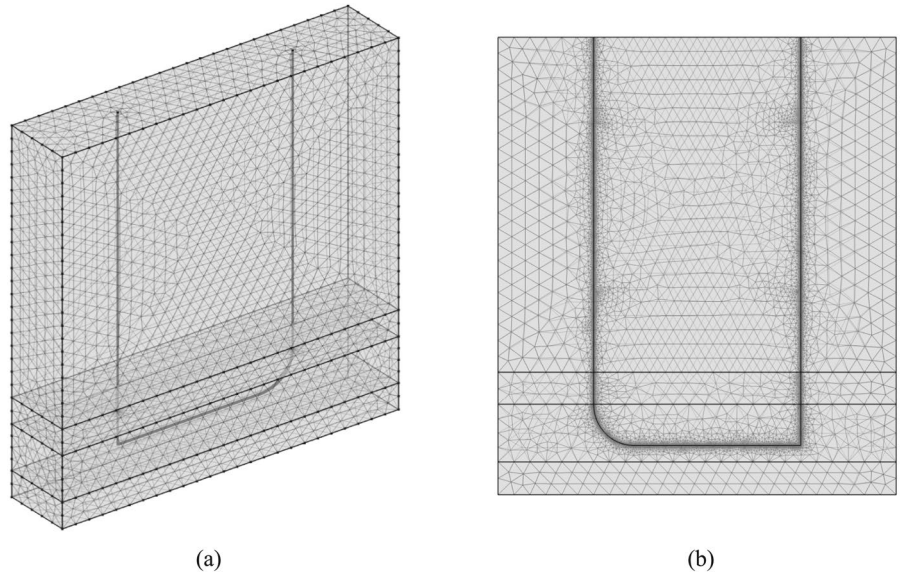

Fig. 4 Finite-element mesh representing the simulation domain of the U-shaped closed-loop geothermal system. **a** A 3-D view of the reservoir model, where the mesh is refined toward the wellbore. **b** A cross section showing the localized refinement around the wellbore, ensuring higher resolution for greater numerical accuracy in region with higher thermal gradient. The reservoir temperature at the lateral depth (5 km) is 195 °C

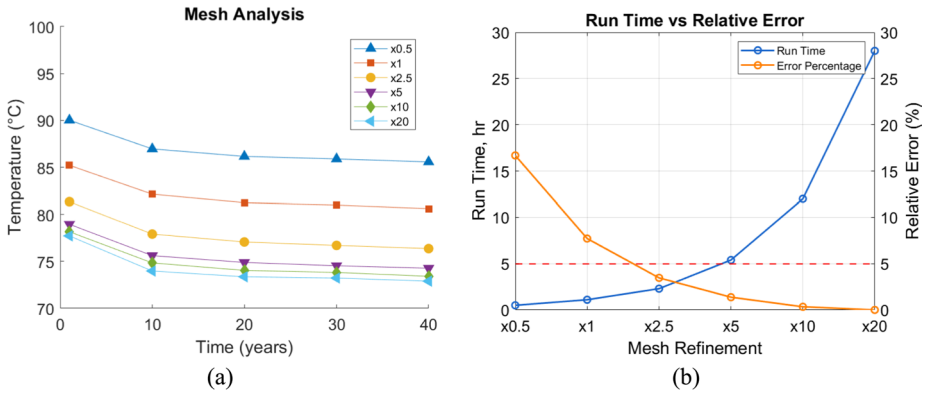

Fig. 5 **a** Temperature profiles with varying mesh densities over a 40-year simulation period. The baseline mesh resolution (×1) corresponds to one element/meter along the wellbore. Subsequent refinements increase the number of elements/meter, with ×0.5 representing a coarser mesh and × 20 a finer mesh. **b** Comparison between computational run time (blue curve) and relative error (orange curve) for different mesh refinements. The mesh refinement ranges from 0.5 to 20 elements/meter along the wellbore, with × 20 taken as the reference solution that others are compared to. The dashed red line represents a 5% error threshold, used as a benchmark for acceptable accuracy

Figure 5a shows the temperature output for the different stages of mesh refinement, starting from courser to finer mesh distribution around the wellbore. The coarser mesh overestimates the amount of heat extracted, with a difference of more than 13 °C as compared to finer mesh. The temperature output drops significantly for initial refinements and starts to converge for a mesh multiplier of 10, whereby the difference between mesh multiplier of 10 and 20 is less than 1 °C.

Figure 5b shows the error analysis and computational time for the different meshing schemes relative to the finest mesh used. A threshold of 5% maximum relative error, calculated relative to the reference solution of 20 elements/meter, is used to identify a suitable mesh resolution, which combines low relative error and reasonable run time. The resulting mesh configuration used for the study is × 2.5 which leads to a total of 279,476 domain elements.

Results

Base case

The base-case scenario, defined in Table 1, serves as a reference solution for evaluating the thermal performance of U-shaped CLGS under variable conditions. Corresponding results reveal a stable and sustained power output over an assumed 40-year operational period (Fig. 6). The net power output starts at 6.3 MW and experiences a rapid decline during the initial transient phase, primarily due to the large thermal gradient between the working fluid in the wellbore and the surrounding formation. This transient phase lasts for less than a year, after which the system stabilizes at a steady average power output of 3.6 MW. The cumulative energy output increases throughout the operational period to reach 4.5×10^9 MJ by year 40. Furthermore, Fig. 6b shows the temperature distribution along the wellbore. The temperature of the working fluid rises progressively as it travels through the U-shaped wellbore. The descending section (red line in Fig. 6b) experiences the most significant temperature increase due to the initial thermal gradient, followed by the horizontal section (blue line in Fig. 6b), where advection and conduction enhance heat uptake from the surrounding formation. In the ascending section (green line in Fig. 6b), the temperature stabilizes as heat exchange slows, reaching a near-constant value before exiting the system.

Moreover, the well design with its different sections and multiple layers of casing and cement introduces thermal resistance along the wellbore depth. Each layer (with its respective properties as listed in Tables 1 and 2) acts as a thermal barrier, influencing the rate at which heat moves from the surrounding formation to the circulating fluid.

Impact of groundwater flow

The influence of groundwater flow on the thermal performance of the U-loop CLGS is analyzed under varying Péclet numbers (Pe) and flow velocities, capturing the shift from conduction-dominated to advection-assisted heat transfer mechanisms, where advective flow enhances conductive heat transfer. Figure 7 shows the temperature distribution around the lateral section of the wellbore at different groundwater velocities, ranging from 0 to 20 m/yr. At 0 m/yr (Pe = 0), the system is conduction-dominated, producing a symmetric thermal plume around the lateral section of the borehole with limited heat transfer enhancement. However, as groundwater velocity increases, the plume extends downstream due to advective heat transport, demonstrating the transition to an advection-assisted regime. The temperature distribution along a 1D line in a horizontal cross-section perpendicular to the wellbore (Fig. 8) further supports this observation. As groundwater velocities increase from 0 m/yr to 20 m/yr, the thermal plume around the lateral wellbore becomes more pronounced and asymmetric with elevated

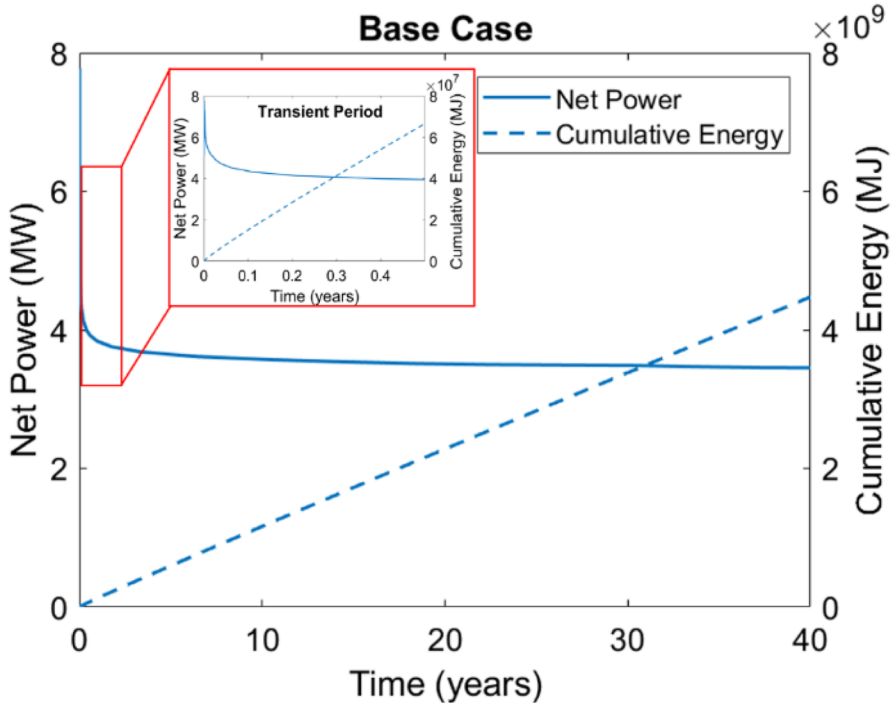

(a)

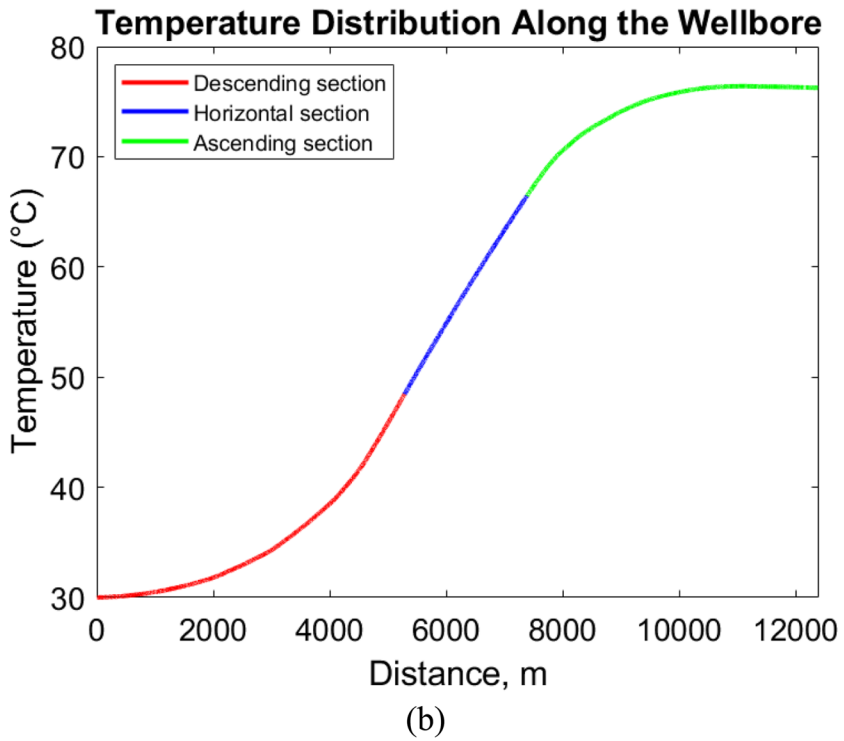

(b)

Fig. 6 **a** Power output (solid line) and cumulative energy (dashed lines) over time for the base case scenario, showing transient and steady-state behavior. **b** Temperature distribution along the wellbore after 40 years, highlighting thermal profiles in the descending, horizontal, and ascending sections

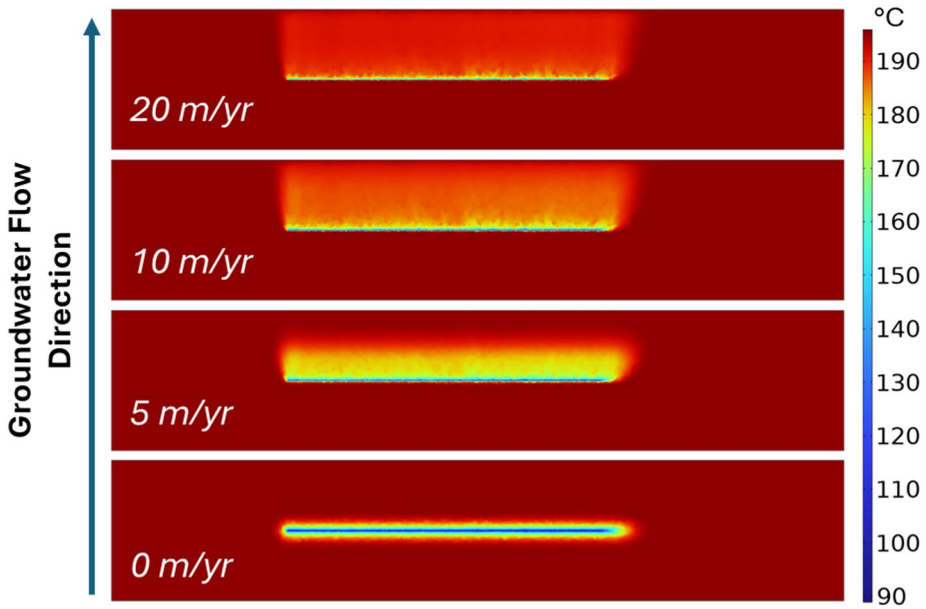

Fig. 7 Temperature distribution along a horizontal cross-section across the lateral section of a U-shaped closed-loop geothermal system (CLGS) under varying groundwater velocities. The three scenarios show the effect of groundwater flow rates on heat dispersion, with velocities of 0, 5, and 10 m/yr (from bottom to top). At lower velocities, the temperature distribution is symmetrical around the lateral section, while higher groundwater flow results in increased advective heat transport that extends the thermal plume

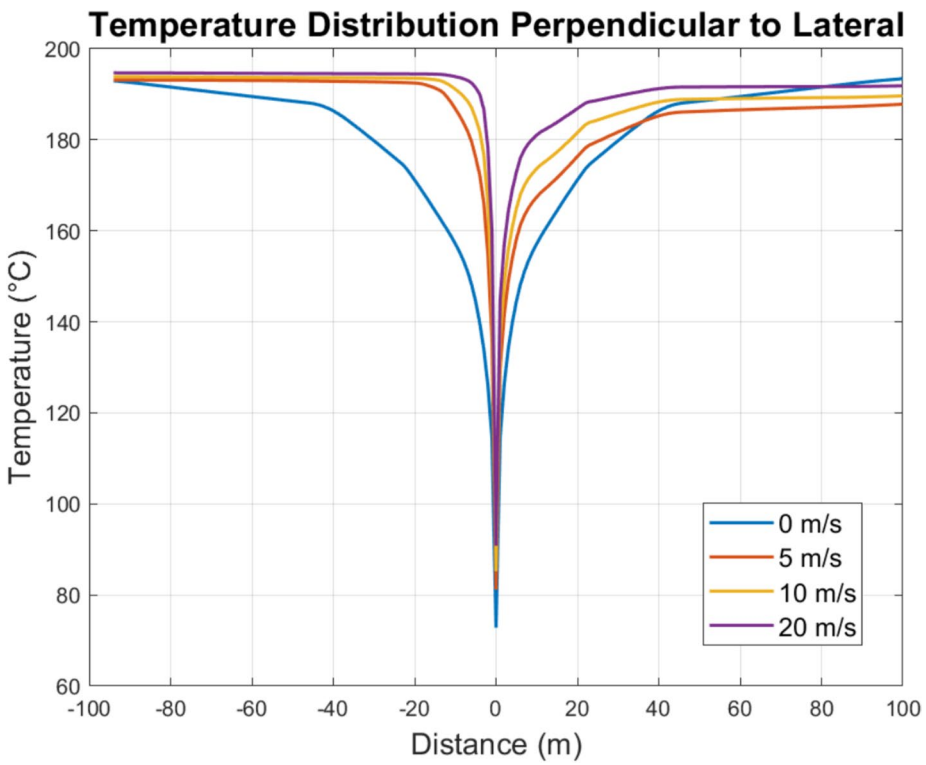

Fig. 8 Temperature distribution along a 1D line perpendicular to the lateral section of the U-shaped wellbore, showing the temperature profiles corresponding to varying groundwater velocities (0, 5, 10, and 20 m/yr). At zero groundwater flow, the temperature field exhibits a symmetric distribution around the wellbore

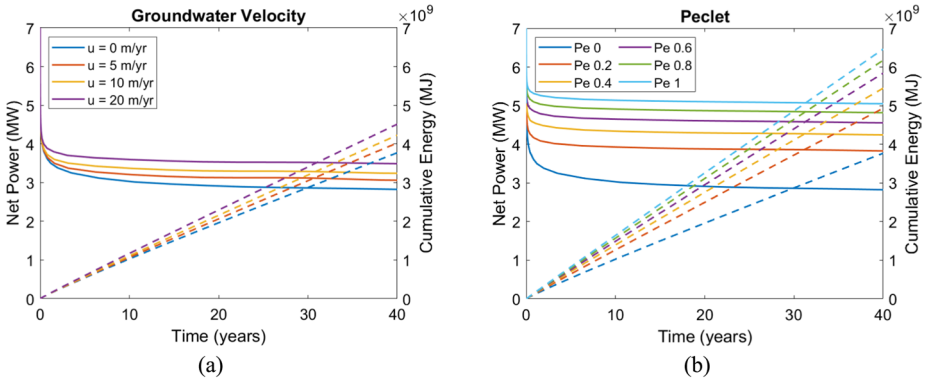

Fig. 9 **a** Effect of groundwater velocity flow (0, 5, 10, and 20 m/yr) on net power (solid line) and cumulative energy (dashed lines), **b** Influence of Peclet numbers (Pe = 0–1) illustrating the role of advective heat transport in system efficiency. Note: zero groundwater velocity corresponds to Pe = 0, while the base-case velocity of 20 m/yr is calculated to have Pe = 0.18

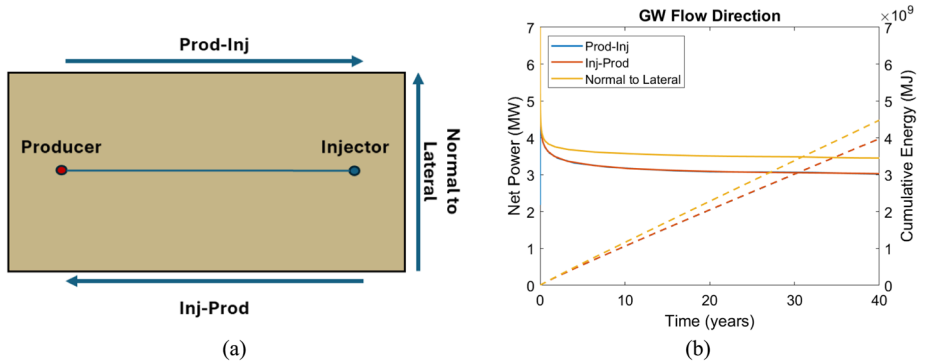

Fig. 10 Scenario modeling of groundwater flow direction. **a** Schematic representation of the groundwater flow direction relative to the lateral section of the U-shaped well, showing the position of the injector and producer. **b** Power output (solid line) and cumulative energy (dashed lines) over time for different groundwater flow directions

temperatures downstream due to advective heat transport. This reduces the extent of the thermal depletion zone, leading to better-sustained heat extraction.

Figure 9 evaluates the impact of groundwater flow velocity on the power output over a 40-year period. With higher groundwater flow velocities (and consequently higher Péclet numbers), power output stabilizes at elevated levels due to the enhanced advective heat recharge surrounding the lateral wellbore, while the cumulative energy production increases proportionally with the groundwater flow, highlighting the long-term benefit of advective heat transport on the system. Relative to the conduction-only scenario, the perpendicular groundwater flow case (20 m/yr) increased cumulative thermal energy output by 27% after 40 years of operation (Fig. 9a).

The alignment of the horizontal (lateral) section of the wellbore relative to the groundwater flow direction further influences the heat transfer efficiency. Figure 10a illustrates the different scenarios for groundwater flow, including flow from producer to injector (parallel alignment), injector to producer (reverse parallel alignment), and perpendicular to the lateral section (normal to lateral). The results in Fig. 10b show that perpendicular

alignment produces the most favorable results. This configuration maximized the heat recharge around the lateral section. In comparison, parallel alignments are less effective due to the reduction in the rate of thermal recharge.

Impact of operational parameters

We vary operational parameters to analyze their influence on thermal and energy performance of the U-loop CLGS. Injection rate and injection temperature variations reveal how they affect system efficiency and thermal output over a 40-year operational period (Fig. 11). Increasing the injection rate initially improves the net power output, with the best performance observed at 30 kg/s (Fig. 11a, b), where the system achieves a steady-state net power output of 3.6 MW. At this flow rate, the combination of increased fluid circulation and adequate residence time maximizes heat absorption from the surrounding rock formation. However, further increasing the injection rate beyond 30 kg/s causes a decline in net power output. At 100 kg/s the net power output drops to 2.3 MW. Two factors contribute to this decline (Fig. 11b). First, higher flow rates reduce the residence time of the working fluid, leading to a smaller temperature difference (ΔT) between the injector and producer, which is evident in the gross power curve (excluding pump losses). Second, the pump energy requirement grows rapidly at high flow rates due to

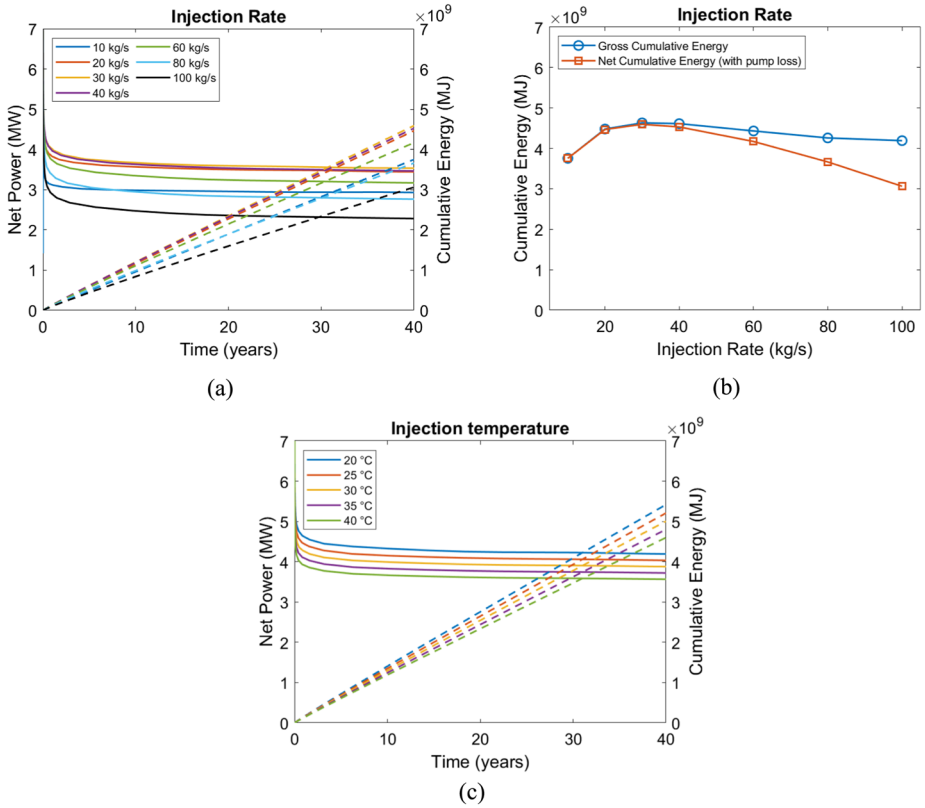

Fig. 11 Impact of injection rate and injection temperature on power output (solid line) and cumulative energy (dashed lines) over a 40-year period. **a**, **b** Effect of varying injection rates (10–100 kg/s). An optimal injection rate of 30 kg/s yields the highest power output, increasing rates beyond that lead to diminishing returns due to increased parasitic pumping losses. **c** Injection temperatures (20–40 °C). Lower injection temperatures enhance heat transfer efficiency by increasing the thermal gradient

higher pressure difference (ΔP), and these parasitic losses offset any benefits from increased circulation. Accounting for both is therefore crucial to ensure that the gains in energy extraction are not offset by excessive operational costs.

Injection temperature can significantly impact system performance by controlling the thermal gradient between the working fluid and the surrounding rock formation. As shown in Fig. 11c, lower injection temperatures result in greater net power output due to a larger thermal gradient that enhances heat transfer efficiency. For example, at injection temperature of 20 °C, the system achieves the highest steady-state net power output of ~ 4.2 MW. In contrast, increasing the injection temperature to 40 °C reduces the thermal gradient, limiting the heat transfer rate. As a result, the net power output decreases to 3.6 MW, and cumulative energy production declines correspondingly.

Impact of geological parameters

Geological parameters, including reservoir depth, geothermal gradient, porosity, and thermal conductivity of the formation play a critical role in the CLGS's overall thermal performance. Reservoir depth and geothermal gradient are interrelated parameters that collectively define the thermal energy available in the subsurface. Greater depths are typically associated with higher temperatures due to the natural geothermal gradient, which represents the rate of temperature increase per unit depth. As shown in Fig. 12a, b, deeper reservoirs (from 3 to 5 km) and higher geothermal gradient (from 25 °C/

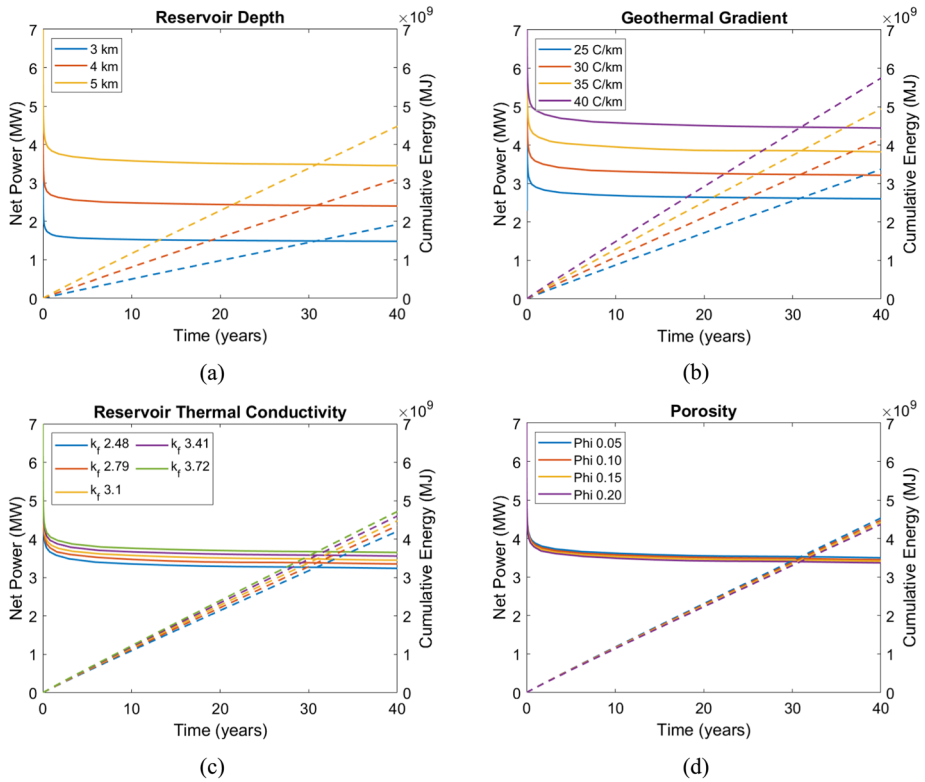

Fig. 12 Influence of key geological parameters on power output (solid line) and cumulative energy (dashed lines) over 40 years. Each subplot focuses on a single parameter including **a** reservoir depth, **b** geothermal gradient, **c** reservoir thermal conductivity, and **d** porosity

km to 40 °C/km) lead to substantial improvement in net power output and cumulative energy production. The thermal energy available in the reservoir increases proportionally with higher depths and geothermal gradients, creating a larger temperature difference between the formation and the working fluid. This elevated gradient increases the rate of heat transfer into the circulating fluid, resulting in improved energy extraction.

For instance, at 5 km depth and a geothermal gradient of 32 °C/km, the net power output reaches 3.5 MW by year 40, significantly higher than found for shallower reservoirs or lower geothermal gradients (Fig. 12b). These results highlight that targeting deeper reservoirs in regions with higher geothermal gradients, assuming negligible change in permeability and porosity, may maximize system performance and long-term energy recovery. However, it is important to balance these benefits against the economic trade-offs of drilling deeper wells, which increases capital costs. Regions with naturally elevated geothermal gradients and advective/convective heat flow, induced by groundwater flow, offer an advantage by providing higher formation temperatures at shallower depths, thereby reducing drilling requirements and costs.

The reservoir's thermal conductivity determines the rate at which heat is transferred from the surrounding rock to the working fluid circulating in the wellbore. As shown in Fig. 12c, increasing this value from 2.5 to 3.7 W/(m·K) markedly enhances system performance. Higher thermal conductivity increases heat transfer, leading to higher net power output and cumulative energy production. For example, at 3.72 W/(m·K), the net power output is 3.7 MW by year 40, compared to 3.2 MW at thermal conductivity of 2.5 W/(m·K). This result underscores the importance of evaluating the reservoir's thermal properties to determine the feasibility and long-term potential of geothermal systems.

Porosity influences effective thermal conductivity and heat capacity of the formation, which in turn affects the heat transfer to the working fluid. Figure 12d shows that increased porosity (from 0.05 to 0.2) leads to a slight reduction in net power output and cumulative energy production. This decrease is attributed to the lower effective thermal conductivity of higher-porosity formations, which reduces the rate of heat transfer to the working fluid.

Impact of well-design parameters

To investigate the effect of well-design parameters on heat and energy output, variations in wellbore size, thermal conductivity of cement, and lateral length are evaluated. The diameter of the horizontal hole section, for instance, directly influences the heat extraction process by increasing the contact area between the working fluid (water) and the wellbore-formation interface. As shown in Fig. 13a, increasing the diameter from 0.114 to 0.245 m results in a steady rise in power output from 3.1 MW to 3.7 MW, respectively, because larger diameters increase the heat transfer surface area, allowing more thermal energy to be absorbed by the working fluid.

Thermal conductivity of the cement, which is situated in wellbore annulus, significantly impacts heat transfer efficiency. Figure 13b shows that increasing its value from 0.2 to 0.8 W/(m·K) raises the net power output by approximately 90%. The cement and casing layers in the wellbore act as a thermal bridge controlling the heat transfer rate from the formation to the working fluid. Therefore, material selection and optimization of the cement is critical in maximizing the heat transfer efficiency in CLGS. Conductive

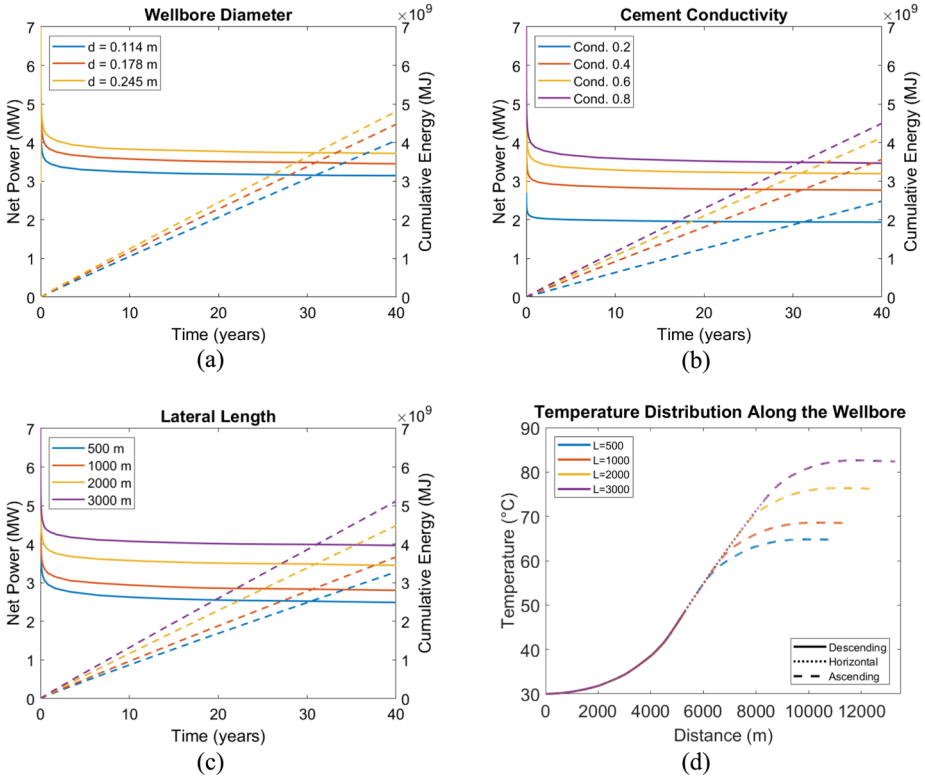

Fig. 13 Influence of key design parameters on power output (solid line) and cumulative energy (dashed lines) over 40 years. Each subplot focuses on a single parameter including, **a** Wellbore diameter, **b** cement thermal conductivity, **c** lateral lengths, and **d** temperature profiles along the descending, horizontal, and ascending wellbore segments for each lateral length

cement can significantly improve energy extraction by ensuring minimal thermal resistance along the wellbore in the deeper, horizontal parts and maximal thermal resistance in the shallower, vertical parts.

Lateral length is another design parameter that affects heat extraction efficiency. Extending the horizontal well section expands the heat exchange area, allowing for greater fluid residence time and more efficient heat extraction. As shown in Fig. 13c, increasing lateral length from 0.5 to 3 km substantially improves system performance. The net power output increases from approximately 2.5 MW at 0.5 km to 4 MW at 3 km. A longer lateral allows the working fluid to absorb heat over a greater distance, maximizing thermal recovery (Fig. 13d).

Sensitivity analysis

To assess the influence of the key parameters on the performance of the U-shaped CLGS, we conduct a local sensitivity analysis, meaning each parameter is varied individually by $\pm 15\%$ relative to its base-case value, while all other parameters are held constant. The effect of these variations on the energy output is then evaluated. The outcome of this sensitivity analysis is depicted in Fig. 14, which shows that geological parameters such as geothermal gradient and reservoir depth exhibit the highest sensitivity, highlighting the importance of careful evaluation of the reservoir properties. Regions with higher

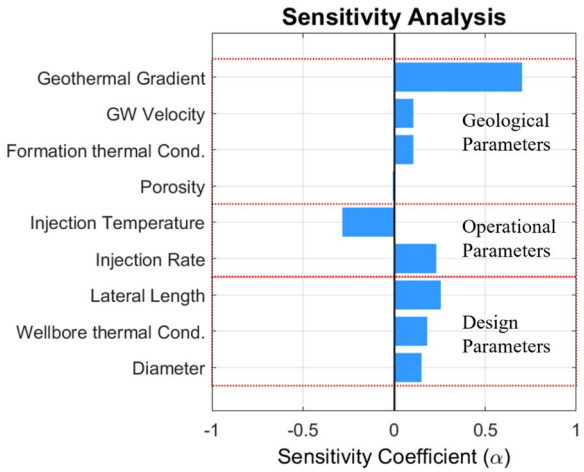

Fig. 14 Sensitivity analysis of key parameters affecting the system's performance. The sensitivity coefficients (α) indicate the relative impact of each parameter, with positive values enhancing and negative values reducing performance

geothermal gradients and favorable reservoir conditions offer substantial thermal energy potential, which directly increases net power output and cumulative energy production. Operational parameters, particularly flow rate, demonstrate the ability to optimize system performance in real time. Adjusting flow rates can enhance power output, but this must be balanced against parasitic pumping power requirements to ensure operational efficiency.

Discussion

Our study highlights the role of groundwater flow in enhancing the thermal performance of U-shaped closed-loop geothermal systems (CLGS). Specifically, introducing advective heat transport driven by groundwater flow increases heat recharge rates near the wellbore, particularly if the lateral section is perpendicular to the flow (Fig. 10). This alignment maximizes advective heat transfer by ensuring continuous replacement of cooler fluid around the lateral part of the wellbore with warmer fluid from surrounding areas, a mechanism consistent with previous work on subsurface heat-exchange under the influence of groundwater flow (Diao et al. 2004; Hecht-Méndez et al. 2013). Our findings show that up to 27% more energy can be extracted if groundwater flow is present. This result is consistent with the recent work by Brown & Falcone (2025) who demonstrated similar improvements in thermal output for single and multilateral U-shaped systems under perpendicular groundwater flow. Our study extends their work by implementing a fully coupled 3D finite-element model that captures detailed well construction (e.g., casing, cement, and insulation layers) and varied geological parameters. In addition, we account for parasitic pumping losses and sensitivity analyses across operational and design parameters, allowing for a more comprehensive evaluation of net power performance. This suggests that sedimentary basins with active groundwater flow are particularly well-suited for the deployment of CLGS in terms of performance and likely cost.

Geological parameters, such as geothermal gradient and reservoir depth determine the thermal energy available for extraction. These parameters are critical for assessing

site feasibility and guiding the initial evaluation for CLGS deployment. These parameters form the foundation for determining whether a given location is suitable for geothermal energy harvesting. Although advective flow in porous media is inherently porosity dependent, the impact of porosity in our simulations appears minor. This is because the groundwater flow is applied as a Darcy velocity boundary condition, meaning groundwater velocity is held constant regardless of porosity variations. By exploring a range of groundwater velocities, our results capture the variability in advective heat transfer that could arise from different porosity values. Moreover, the rock matrix dominates the effective thermal properties, as geological materials typically exhibit higher thermal conductivity and lower volumetric heat capacity than water (Dehkordi & Schincariol 2014; Nield & Bejan 2017b). As a result, porosity primarily affects the conductive component of heat transfer, which is less significant under advective conditions. This explains the limited sensitivity of the system's performance to porosity in our results (Figs. 12d, 14).

Operational parameters such as injection rates and injection temperature play a critical role in optimizing the system's performance. In general, lower injection temperatures improve heat transfer efficiency. However, the minimum injection temperature is typically constrained by the surface application, as it must remain consistent with realistic operational conditions. Injection rates, on the other hand, require careful management to avoid excessive parasitic pumping power while maximizing energy output. For instance, the optimal injection rate for the base case scenario was identified as 30 kg/s (Fig. 11) to balance heat extraction efficiency with manageable parasitic pumping power. Our results are thus consistent with the findings of Ma et al. (2023) and Liu & Dahi Taleghani (2023) who demonstrated how injection rates and temperature can be used to enhance the overall heat extraction performance of U-shaped geothermal systems. Similarly, design parameters like lateral length and wellbore diameter significantly affect heat extraction efficiency by increasing fluid residence time and expanding heat exchange areas. However, factors such as the capital costs associated with drilling deeper wells, increasing wellbore diameters, and extending laterals must be carefully evaluated during the design and operational planning stages to balance maximizing performance and maintaining economic viability (Beckers et al. 2022).

The sensitivity analysis (Fig. 14) reveals that geological parameters, such as geothermal gradient and reservoir depth, have the most significant influence on system performance. These parameters directly impact the thermal energy available for extraction, making regions with high geothermal gradients or greater depths particularly favorable for CLGS deployment. Among operational parameters, the injection rate proved critical; while higher rates improve net power output, they necessitate careful management to avoid excessive parasitic pumping power. Design parameters, including lateral well length and wellbore diameter, are also identified as key contributors to enhanced heat extraction, demonstrating the importance of optimizing these features during the planning phase.

From a deployment standpoint, the results suggest sedimentary basins with measurable hydraulic gradients are promising for U-loop CLGS. Performance is maximized if the lateral well is oriented perpendicular to the dominant groundwater flow direction. In practice, this implies a simple workflow: (1) screen gradient-depth windows (e.g. Figures 12, 14) to assess thermal potential; (2) measure pressure gradients/hydraulic

conductivity to estimate Pe; (3) design lateral orientation and length to capture advective recharge while respecting drilling and completion constraints; and (4) optimize injection temperature/rate to maximize net power output.

Our study offers important insights for developing a closed-loop geothermal system in a sedimentary based, but certain limitations apply. For instance, the presence and velocity of groundwater flow in the Midyan basin remain uncertain due to the lack of direct measurements. The assumed base-case porosity and permeability values represent a moderately porous sedimentary formation but may be optimistic at 5 km depth. At such depths, porosity and permeability may be lower. Because compaction behavior under high mean stress varies appreciably for siliclastic sedimentary rocks (Lee et al. 2020), only laboratory measurements conducted on site-specific core plugs can better constrain these values. Although the sensitivity analysis covers a reasonable range, future studies should incorporate depth- and stress-corrected data where available. Furthermore, the model assumes homogenous matrix flow and does not account for natural fractures or faults that may channelize groundwater flow and influence thermal recharge.

From a well-construction perspective, completing U-shaped wells to depths of ~ 5 km remains technically challenging. However, the recent modeling studies have demonstrated their feasibility (White et al. 2024), and advances in directional drilling technologies, such as push-the-bit rotary steerable systems, allow precise wellbore placement with minimal vertical and lateral deviations (Garda 2024). To support the practical deployment of CLGS in sedimentary formations, we recommend the acquisition of detailed geological and hydrological data, including pressure gradients and hydraulic conductivity from core plugs, and possibly tracer tests to detect flow pathways. Such data are critical for confirming the presence, magnitude, and direction of groundwater flow.

Conclusions

Integrating groundwater flow into the U-loop closed-loop geothermal systems (CLGS) numerical model revealed a transition from conduction-dominated to advection-assisted heat transfer regimes, significantly impacting system efficiency and long-term energy production. Key findings of our study include:

- The presence of groundwater flow replenishes heat around the wellbore, effectively increasing the in situ thermal recharge. This continuous influx of warmer fluid enhances the heat transfer process and energy output compared to conduction-only scenarios, indicating that such geological settings are particularly well-suited for the application of CLGS.
- Orienting the lateral section of the U-shaped wellbore perpendicular to the direction of groundwater flow maximizes advective heat transfer. This alignment ensures a continuous influx of warmer fluid that effectively replaces cooler fluid along the entire lateral section, thereby optimizing thermal recharge and power output.
- Geothermal gradient and reservoir depth exert the strongest influence on system performance. Higher gradients and deeper reservoirs increase the available thermal

energy, emphasizing the need for thorough reservoir evaluation during site selection phase.

- Our study identifies an optimal injection rate (e.g., 30 kg/s in the base-case scenario) that maximizes net power output while maintaining efficient operation. Increasing the injection rate beyond 30 kg/s decreases the net power output due to higher parasitic pumping requirements.
- Increasing the lateral wellbore length and diameter improves heat transfer efficiency and higher power output. However, capital costs associated with design parameters must be considered to ensure economic feasibility.

In summary, our research provides a framework for evaluating CLGS performance under dynamic hydrological conditions, contributing valuable insights for geothermal energy development in deep sedimentary basins.

Acknowledgements
We thank the four anonymous reviewers and the Associate Editor for the constructive criticism and detailed comments that helped to improve the quality of our manuscript. We also thank the ENOWA geothermal team at NEOM for stimulating discussions and motivating this study.

Author contributions
O.A.: Conceptualization, methodology, software, formal analysis, investigation, writing – original draft, writing – review & editing. J.E.: Conceptualization, methodology, formal analysis, writing – review & editing. a.D.: Software, methodology, formal analysis, writing – review & editing. T.F.: Methodology, formal analysis, writing – review & editing. P.M.: Conceptualization, methodology, review & editing, financial & logistic support.

Funding
The authors would like to acknowledge King Abdullah University of Science and Technology (KAUST) for supporting this researcher under grants BAS/1/1339–01-01 (PMM), REI/1/4502–01-01 and RGC/3/5229–01-01 (CJE and PMM), and Saudi Aramco for funding the PhD studies of O. Alobaid (OMA).

Data availability
No datasets were generated or analysed during the current study.

Declarations

Ethics approval and consent to participate
Not applicable.

Competing interests
The authors declare no competing interests.

Received: 16 April 2025 Accepted: 4 October 2025
Published online: 27 October 2025

References

Barnard ACL, Hunt WA, Timlake WP, Varley E. A theory of fluid flow in compliant tubes. Biophys J. 1966;6(6):717–24. https://doi.org/10.1016/S0006-3495(66)86690-0.
Bear J. Dynamics of fluids in porous media. 1972
Beckers KF, Rangel-Jurado N, Chandrasekar H, Hawkins AJ, Fulton PM, Tester JW. Techno-economic performance of closed-loop geothermal systems for heat production and electricity generation. Geothermics. 2022. https://doi.org/10.1016/j.geothermics.2021.102318.
Brown CS, Falcone G. Investigating the impact of groundwater flow on multi-lateral, U-type, advanced geothermal systems. Appl Therm Eng. 2025;271:126269. https://doi.org/10.1016/j.applthermaleng.2025.126269.
Chettri N, Sankarananth S. Geothermal energy: definition and its applications. Technoarete Trans Renew Energy Green Energy Sustain. 2022;2:12–7.
Churchill SW. Friction-factor equation spans all fluid-flow regimes. Chem Eng. 1977;84(24):91–2.
Coulson JM, Richardson JF, Backhurst JR, Harker JH. Fluid flow, heat transfer and mass transfer. In Heat transfer and mass transfer. 1990
Daniilidis A. Towards comprehensive uncertainty quantification in direct-use geothermal systems. 85th EAGE Ann Conf Exhibit. 2024. https://doi.org/10.3997/2214-4609.2024101678.

Dehkordi SE, Schincariol RA. Effect of thermal-hydrogeological and borehole heat exchanger properties on performance and impact of vertical closed-loop geothermal heat pump systems. Hydrogeol J. 2014;22(1):189–203. https://doi.org/10.1007/s10040-013-1060-6.
Diao N, Li Q, Fang Z. Heat transfer in ground heat exchangers with groundwater advection. Int J Therm Sci. 2004;43(12):1203–11. https://doi.org/10.1016/j.ijthermalsci.2004.04.009.
Ezekiel J, Ebigbo A, Arifianto I, Daniilidis A, Finkbeiner T, Mai PM. Techno-economic performance optimization of hydrothermal doublet systems: application to the Al Wajh basin, Western Saudi Arabia. Geothermics. 2022. https://doi.org/10.1016/j.geothermics.2022.102532.
Garda I. A sustainable path forward: delivering Canada's longest montney lateral. SPE Annual Technical Conference and Exhibition. 2024. https://doi.org/10.2118/221064-MS
Ghassemi A, Zhang Q. A transient fictitious stress boundary element method for porothermoelastic media. Eng Anal Boundary Elem. 2004;28(11):1363–73. https://doi.org/10.1016/j.enganabound.2004.05.003.
Gössling S, Peeters P, Hall CM, Ceron JP, Dubois G, Lehmann LV, et al. Tourism and water use: supply, demand, and security. An international review. Tour Manage. 2012;33(1):1–15. https://doi.org/10.1016/J.TOURMAN.2011.03.015.
Gude VG. Desalination and sustainability – an appraisal and current perspective. Water Res. 2016;89:87–106. https://doi.org/10.1016/J.WATRES.2015.11.012.
Hecht-Méndez J, De Paly M, Beck M, Bayer P. Optimization of energy extraction for vertical closed-loop geothermal systems considering groundwater flow. Energy Convers Manage. 2013;66:1–10. https://doi.org/10.1016/j.enconman.2012.09.019.
Huang S, Li J, Zhu K, Dong J, Jiang Y. Numerical investigation on the long-term heating performance and sustainability analysis of medium-deep U-type borehole heat exchanger system. Energy. 2024. https://doi.org/10.1016/j.energy.2023.129955.
Hughes GW, Johnson RS. Lithostratigraphy of the Red Sea region. In 49 GeoArabia. 2005. 10(13). http://pubs.geoscienceworld.org/gpl/geoarabia/article-pdf/10/3/49/5442127/hughes.pdf
Huysmans M, Dassargues A. Review of the use of Péclet numbers to determine the relative importance of advection and diffusion in low permeability environments. Hydrogeol J. 2005;13(5–6):895–904. https://doi.org/10.1007/s10040-004-0387-4.
IEA. (2023). World energy outlook 2023. www.iea.org/reports/world-energy-outlook-2023
Kamila Z, Kaya E, Zarrouk SJ. Reinjection in geothermal fields: an updated worldwide review 2020. Geothermics. 2021. https://doi.org/10.1016/j.geothermics.2020.101970.
Kraft T, Mai PM, Wiemer S, Deichmann N, Ripperger J, Kästli P, Bachmann C, Fäh D, Wössner J, Giardini D. Enhanced geothermal systems: Mitigating risk in urban areas. Eos, Transactions American Geophysical Union. 2009 Aug 11;90(32):273-4. https://doi.org/10.1029/2009EO320001
Lee EY, Novotny J, Wagreich M. Compaction trend estimation and applications to sedimentary basin reconstruction (BasinVis 2.0). Appl Comput Geosci. 2020. https://doi.org/10.1016/j.acags.2019.100015.
Limberger J, Boxem T, Pluymaekers M, Bruhn D, Manzella A, Calcagno P, et al. Geothermal energy in deep aquifers: a global assessment of the resource base for direct heat utilization. Renew Sustain Energy Rev. 2018;82:961–75. https://doi.org/10.1016/j.rser.2017.09.084.
Liu S, Dahi Taleghani A. Analysis of an enhanced closed-loop geothermal system. Geoenerg Sci Eng. 2023;231:212296. https://doi.org/10.1016/J.GEOEN.2023.212296.
Liu S, Liu J, Chai J, Xue Y, Liu J, Bai X. Design and optimization of the U-shaped well geothermal systems for heat production performance: A case study from Huangling, China. Renewable Energy. 2024 Mar 1;223:120060.
Lucazeau F. Analysis and mapping of an updated terrestrial heat flow data set. Geochem Geophys Geosyst. 2019;31(20):4001–24. https://doi.org/10.1029/93RG01249.
Lund JW, Toth AN. Direct utilization of geothermal energy 2020 worldwide review. Geothermics. 2021. https://doi.org/10.1016/j.geothermics.2020.101915.
Lurie MV. Fundamentals of mathematical modeling of one-dimensional flows of fluid and gas in pipelines. In: Modeling of oil product and gas pipeline transportation. Hoboken: Wiley; 2008. p. 1–30.
Ma Y, Li S, Zhang L, Liu S, Wang M. Heat extraction performance evaluation of U-shaped well geothermal production system under different well-layout parameters and engineering schemes. Renew Energy. 2023;203:473–84. https://doi.org/10.1016/j.renene.2022.12.082.
Majer EL, Baria R, Stark M, Oates S, Bommer J, Smith B, et al. Induced seismicity associated with enhanced geothermal systems. Geothermics. 2007;36(3):185–222. https://doi.org/10.1016/J.GEOTHERMICS.2007.03.003.
Malek AE, Adams BM, Rossi E, Schiegg HO, Saar MO. Techno-economic analysis of advanced geothermal systems (AGS). Renew Energy. 2022;186:927–43. https://doi.org/10.1016/j.renene.2022.01.012.
Maliva, Robert G. Aquifer characterization techniques. Vol. 10. Berlin: Springer, 2016.
Moeck IS. Catalog of geothermal play types based on geologic controls. Renew Sustain Energy Rev. 2014;37:867–82. https://doi.org/10.1016/j.rser.2014.05.032.
Nield DA, Bejan A. Convection in porous media. Cham: Springer International Publishing; 2017. https://doi.org/10.1007/978-3-319-49562-0.
Ouerghi FH, Omri M, Nisar KS, Abd El-Aziz RM, Taloba AI. Investigating the potential of geothermal energy as a sustainable replacement for fossil fuels in commercial buildings. Alexandria Eng J. 2024;97:215–29. https://doi.org/10.1016/J.AEJ.2024.03.094.
Pratiwi AS, Trutnevyte E. Life cycle assessment of shallow to medium-depth geothermal heating and cooling networks in the state of Geneva. Geothermics. 2021. https://doi.org/10.1016/j.geothermics.2020.101988.
Rathnaweera TD, Wu W, Ji Y, Gamage RP. Understanding injection-induced seismicity in enhanced geothermal systems: from the coupled thermo-hydro-mechanical-chemical process to anthropogenic earthquake prediction. Earth-Sci Rev. 2020. https://doi.org/10.1016/j.earscirev.2020.103182.
Schill E, Meixner J, Meller C, Grimm M, Grimmer JC, Stober I, et al. Criteria and geological setting for the generic geothermal underground research laboratory, GEOLAB. Geotherm Energy. 2016. https://doi.org/10.1186/s40517-016-0049-5.

Song X, Shi Y, Li G, Shen Z, Hu X, Lyu Z, et al. Numerical analysis of the heat production performance of a closed loop geothermal system. Renew Energy. 2018;120:365–78. https://doi.org/10.1016/j.renene.2017.12.065.
Statista. Distribution of electricity generation worldwide in 2023, by energy source. 2023
Tubbs RE, Fouda HGA, Afifi AM, Raterman NS, Hughes GW, Fadolalkarem YK. Midyan Peninsula, northern Red Sea, Saudi Arabia: seismic imaging and regional interpretation. GeoArabia. 2014. https://doi.org/10.2113/geoarabia1903165.
Ürge-Vorsatz D, Cabeza LF, Serrano S, Barreneche C, Petrichenko K. Heating and cooling energy trends and drivers in buildings. Renew Sustain Energy Rev. 2015;41:85–98. https://doi.org/10.1016/J.RSER.2014.08.039.
Wang J, Azam W. Natural resource scarcity, fossil fuel energy consumption, and total greenhouse gas emissions in top emitting countries. Geosci Front. 2024. https://doi.org/10.1016/j.gsf.2023.101757.
Wang Y, Voskov D, Daniilidis A, Khait M, Saeid S, Bruhn D. Uncertainty quantification in a heterogeneous fluvial sandstone reservoir using GPU-based monte carlo simulation. Geothermics. 2023. https://doi.org/10.1016/j.geothermics.2023.102773.
White M, Vasyliv Y, Beckers K, Martinez M, Balestra P, Parisi C, et al. Numerical investigation of closed-loop geothermal systems in deep geothermal reservoirs. Geothermics. 2024. https://doi.org/10.1016/j.geothermics.2023.102852.
Yalcin B, Ezekiel J, Mai PM. Potential for CO2 plume geothermal and CO2 storage in an onshore Red Sea Rift basin, Al-Wajj, Saudi Arabia: 3d reservoir modeling and simulations. Geothermics. 2024. https://doi.org/10.1016/j.geothermics.2024.102966.
Yolcubal I, Brusseau ML, Artiola JF, Wierenga P, Wilson LG. Environmental physical properties and processes. Environmental monitoring and characterization. 2004:207-39.
Yu C, Zhang Y, Tan Y, Song X, Wang G, Huang H, et al. Simulation study of novel methods for water reinjection efficiency improvement of a doublet system in Guantao sandstone geothermal reservoir. Geothermics. 2023. https://doi.org/10.1016/j.geothermics.2023.102709.
Yuan W, Chen Z, Grasby SE, Little E. Closed-loop geothermal energy recovery from deep high enthalpy systems. Renew Energy. 2021;177:976–91. https://doi.org/10.1016/j.renene.2021.06.028.
Zang A, Oye V, Jousset P, Deichmann N, Gritto R, McGarr A, et al. Analysis of induced seismicity in geothermal reservoirs – an overview. Geothermics. 2014;52:6–21. https://doi.org/10.1016/J.GEOTHERMICS.2014.06.005.

Publisher's Note

Springer Nature remains neutral with regard to jurisdictional claims in published maps and institutional affiliations.